Title

Electrokinetic pumping effects of charged porous media in microchannels using the lattice Poisson-Boltzmann method.

Journal

Journal of colloid and interface science, 304(1)

ISSN

0021-9797

Authors

Wang, Moran
Wang, Jinku
Chen, Shiyi
et al.

Publication Date

2006-12-01

Peer reviewed

Available online at www.sciencedirect.com
ScienceDirect
Journal of Colloid and Interface Science 304 (2006) 246–253
JOURNAL OF Colloid and Interface Science
www.elsevier.com/locate/jcis

Electrokinetic pumping effects of charged porous media in microchannels using the lattice Poisson–Boltzmann method

Moran Wang [a,c,*], Jinku Wang [b], Shiyi Chen [c,d], Ning Pan [a]

[a] *Department of Biological and Agricultural Engineering, University of California, Davis, CA 95616, USA*
[b] *School of Aerospace, Tsinghua University, Beijing 100084, PR China*
[c] *Department of Mechanical Engineering, Johns Hopkins University, Baltimore, MD 21218, USA*
[d] *College of Engineering, Peking University, Beijing 100871, PR China*

Received 18 July 2006; accepted 24 August 2006

Available online 30 August 2006

Abstract

The electrokinetic pumping characteristics of nanoscale charged porous media packed in microchannels are investigated using a mesoscopic evolution method. When the pore size of porous media is comparable to the thickness of electric double layer, the effects of particle surface potentials on the bulk electric potential distribution will not be negligible. The lattice Poisson–Boltzmann method provides an accurate numerical solution for such problems, which combines two sets of lattice evolution methods solving the nonlinear Poisson–Boltzmann equation for electric potential distribution and the Navier–Stokes equations for fluid flow, respectively. The effects of the finite particle size, the bulk ionic concentration, the external electric field strength and the surface potentials on the electroosmotic micropump performances are therefore studied. The results show that for a certain porosity the maximum pumping pressure is inversely proportional to the particle diameter and the flow rate under zero pressure drop increases with the particle size. The pumping flow rate decreases with the backpressure yet increases with the external electric field strength, linearly respectively. The averaged flow rate increases with the bulk ionic concentration and the particle surface potential, but is slightly influenced by the surface potentials of channel walls. The numerical results agree with the published experimental data while some results deviate from the predictions based on the macroscopic linear assumptions.

Keywords: Electrokinetic effect; Micropump; Lattice Poisson–Boltzmann method; Porous media

1. Introduction

Micro- and nano-fluidic devices have gained much recent attention due to their increasing applications in chemical analysis [1], biological and medical diagnostics [2,3], and energy supply [4]. The inherent advantages of miniaturization lie in the integration of complex multi-functions with remaining precise controlling of objects [5,6]. Actuating without any moving parts is a new promising direction for micro-system designs despite the low efficiency [7–10]. Electrokinetic flow (EKF) is one of the most important non-mechanical techniques for micro- and nano-fluidics [10–12], and has been widely applied for pumping [13,14], mixing [15,16], and separating [3] for years. Recently, charged porous media structures have been employed in micro devices to change the fluid behavior. A low flow rate together with a high pumping pressure is therefore obtained, which has been used in capillary electrochromatography (CE) [17] and improved high-performance micropumps [18–20]. With the polarization effect of porous electrodes considered, the structured electrode arrays can be designed as a concentration demixer of electrolytes [21].

Electrokinetic transport phenomena in porous media have been studied much in the past ten years both theoretically and numerically [22–26]. However, most results were actually based on linearization approximations of the Poisson–Boltzmann equation [27] so that the reliable applications were limited to where the electric double layer (EDL) length was

* Corresponding author.
E-mail address: mmwang@ucdavis.edu (M. Wang).

0021-9797/$ – see front matter
doi:10.1016/j.jcis.2006.08.050

very thin or very thick comparing to the channel size. To our knowledge, there is only a public literature that presents successful numerical simulations for the electrokinetic flows in charged porous media by solving the nonlinear Poisson–Boltzmann equation and Navier–Stokes equations [28,29], though the CFD techniques have been successfully applied for channel electrokinetic flows [30–33], even in rough channels [34,35]. For the electrokinetic flows in microchannels packed with charged porous media, the EDL length could be of the same level as the pore size. As a result, the surface charges of particles affect significantly the potential distribution across the channel and therefore affect the flow behavior. If the wall surface potentials of either channel or particles are not very low (>30 mV), the linear approximation for the Poisson–Boltzmann equation will introduce errors into the numerical predictions [31,36]. The nonlinear factor will cause the classical CFD solutions for electrokinetic flows in porous media to be very expensive.

In recent years, a mesoscopic statistics-based method, lattice Boltzmann method (LBM), has been developed for electrokinetic transports in micro devices [18–22]. He and Li [37] proposed a lattice Boltzmann scheme for analyzing the electrochemical processes in an electrolyte based on a locally electrically neutral assumption [38]. Li et al. [39–41] simulated the electrokinetic flows in microchannels using a lattice Boltzmann method with one-dimensional linearized solution of the Poisson–Boltzmann equation. Melchionna and Succi [42] solved the nonlinear Poisson–Boltzmann equation by an efficient multi-grid technique and then predicted the flow behavior using a lattice Boltzmann scheme. The multi-grid technique has great efficiency to solve the nonlinear Poisson–Boltzmann equation; however it has rarely been extended for complex geometries [43,44]. Recently, Guo et al. [45] presented a finite-difference-based lattice Boltzmann algorithm for electroosmotic flows with the Joule heating effect. Wang et al. [46,47] developed a lattice Poisson–Boltzmann method (LPBM) which combined a potential evolution method on discrete lattices to solve the nonlinear Poisson–Boltzmann equation with a density evolution method on discrete lattices to solve the Boltzmann–BGK equation. The LPBM has been applied to study the mixing enhancement in heterogeneously charged microchannels [48] and the roughness and cavitation effects in electroosmotic microfluidics [49].

This paper models and analyzes the electrokinetic pumping effects of charged nanoscale porous media packed in microchannels using the lattice Poisson–Boltzmann method. The effect of particle surface potential on the electric potential distribution is considered by solving the nonlinear Poisson–Boltzmann equation in the whole domain. The enhanced pumping performances by adding the charged porous media are therefore discussed. Several factors are concerned including the particle size, the bulk ionic concentration, the external electric field strength, and the surface potentials of walls and particles. The simulation results will be compared with existing experimental data and macroscopic theories.

2. Numerical model

2.1. Governing equations

For an incompressible laminar flow, the continuity and momentum equations are

$$\nabla \cdot \mathbf{u} = 0, \tag{1}$$

$$\rho \frac{\partial \mathbf{u}}{\partial t} + \rho \mathbf{u} \cdot \nabla \mathbf{u} = -\nabla P + \mu \nabla^2 \mathbf{u} + \mathbf{F}_{\mathrm{E}}, \tag{2}$$

where $\mathbf{u}$ is velocity vector, ρ the solution density, P the pressure, μ the dynamic fluid viscosity and $\mathbf{F}_{\mathrm{E}}$ the electric force density vector. In general, the electrical force in electrokinetic fluids can be expressed as

$$\mathbf{F}_{\mathrm{E}} = \mathbf{F}_{\mathrm{ext}} + \rho_e(\mathbf{E}_{\mathrm{int}} + \boldsymbol{\xi} \times \mathbf{B}_{\mathrm{int}}) + \mathbf{F}_{\mathrm{V}}, \tag{3}$$

where $\mathbf{F}_{\mathrm{ext}}$ represents the external field body forces, including the Lorentz force associated with any externally applied electric and magnetic field. For only an electrical field, $\mathbf{F}_{\mathrm{ext}} = \rho_e \mathbf{E}$, where ρ_e is the net charge density and $\mathbf{E}$ is the electrical field strength. $\mathbf{E}_{\mathrm{int}}$ and $\mathbf{B}_{\mathrm{int}}$ are internally smoothed electrical and magnetic fields due to the motion of the charged particles inside the fluid. $\mathbf{F}_{\mathrm{V}}$ is a single equivalent force density due to the intermolecular attraction [40].

Electric double layer (EDL) theory [27] relates the electrostatic potential and the distribution of counterions and co-ions in the bulk solution by the Poisson equation as follows:

$$\nabla^2 \psi = -\frac{\rho_e}{\varepsilon \varepsilon_0}, \tag{4}$$

where ψ is the electrical potential, ε the dimensionless dielectric constant of the solution, ε_0 the permittivity of a vacuum, and ρ_e the net charge density.

The transport of each ion species is generally determined by the Nernst–Planck equation [50–52]. According to the classical EDL theory, for the dilute solution of point ions where the sizes and interactions of ions are negligible, the equilibrium Boltzmann distribution function can be used to describe the ionic number concentration [53]. Therefore, the net charge density distribution can be expressed as the sum of all the ions in the solution:

$$\rho_e = \sum_i z_i e n_{i,\infty} \exp\left(-\frac{z_i e}{k_{\mathrm{B}} T} \psi\right), \tag{5}$$

where the subscript i represents the ith species, n_∞ is the bulk ionic number concentration, z the valence of the ions (including the sign), e the absolute value of one proton charge, k_{B} the Boltzmann constant, and T the absolute temperature.

Substituting Eq. (5) into Eq. (4) yields the nonlinear Poisson–Boltzmann equation for the electrical potential in the dilute electrolyte solution:

$$\nabla^2 \psi = -\frac{1}{\varepsilon \varepsilon_0} \sum_i z_i e n_{i,\infty} \exp\left(-\frac{z_i e}{k_{\mathrm{B}} T} \psi\right). \tag{6}$$

2.2. Evolution equations

2.2.1. Evolution equation for hydrodynamics

The continuity and momentum equations can be solved by tracking the movements of molecule ensembles through the evolution of the distribution function [54] using the popular lattice Boltzmann method. The lattice Boltzmann equation can be derived from the Boltzmann equation [55]. For the flows with external forces, the continuous Boltzmann–BGK equation with an external force term, F, is

$$\frac{Df}{Dt} \equiv \partial_t f + (\boldsymbol{\xi}\cdot\nabla) f = -\frac{f - f^{\mathrm{eq}}}{\tau_\nu} + F, \tag{7}$$

where $f \equiv f(x, \boldsymbol{\xi}, t)$ is the single particle distribution function in the phase space $(x, \boldsymbol{\xi})$, $\boldsymbol{\xi}$ the microscopic velocity, τ_ν the relaxation time, and f^{eq} the Maxwell–Boltzmann equilibrium distribution. For a steady fluid immersed in a conservative force field, the equilibrium distribution function is defined by adding a Boltzmann factor to the Maxwell–Boltzmann distribution:

$$f^{\mathrm{eq}} = \frac{\rho_0}{(2\pi RT)^{D/2}} \exp\left(-\frac{U}{kT}\right) \exp\left(-\frac{(\boldsymbol{\xi}-\mathbf{u})^2}{2RT}\right), \tag{8}$$

where U is the potential energy of the conservative force field, ρ_0 the fluid density where U lowest, R the ideal gas common constant, D the dimension of the calculation space (1D, 2D, or 3D), k the Boltzmann constant, and $\mathbf{u}$ the macroscopic velocity. Here the external force term, F, needs to be chosen carefully. Dimensional analysis led to the following form of F:

$$F = \frac{\mathbf{G}\cdot(\boldsymbol{\xi}-\mathbf{u})}{RT} f^{\mathrm{eq}}, \tag{9}$$

with $\mathbf{G}$ being the external force per unit mass [56]. The Chapman–Enskog expansion can be used to transform the Boltzmann–BGK equation, Eq. (7), into the correct continuum Navier–Stokes equations [57].

For the two-dimensional case, third-order Gauss–Hermite quadrature leads to the nine-speed LBE model with the discrete velocities

$$\mathbf{e}_\alpha = \begin{cases} (0,0), & \alpha = 0, \\ (\cos\theta_\alpha, \sin\theta_\alpha)c, & \theta_\alpha = (\alpha-1)\pi/2, \\ & \alpha = 1,2,3,4, \\ \sqrt{2}(\cos\theta_\alpha, \sin\theta_\alpha)c, & \theta_\alpha = (\alpha-5)\pi/2 + \pi/4, \\ & \alpha = 5,6,7,8, \end{cases} \tag{10}$$

where c is the sound speed and the density equilibrium distribution

$$f_\alpha^{\mathrm{eq}} = \omega_\alpha \rho_0 \exp\left(-\frac{U}{kT}\right)\left[1 + 3\frac{\mathbf{e}_\alpha\cdot\mathbf{u}}{c^2} + 9\frac{(\mathbf{e}_\alpha\cdot\mathbf{u})^2}{c^4} - \frac{3\mathbf{u}^2}{2c^2}\right], \tag{11}$$

with

$$\omega_\alpha = \begin{cases} 4/9, & \alpha = 0, \\ 1/9, & \alpha = 1,2,3,4, \\ 1/36, & \alpha = 5,6,7,8. \end{cases} \tag{12}$$

Thus, the discrete density distribution satisfies the evolution equation

$$f_\alpha(\mathbf{r} + \mathbf{e}_\alpha\delta_t, t+\delta_t) - f_\alpha(\mathbf{r}, t) = -\frac{1}{\tau_\nu}\left[f_\alpha(\mathbf{r}, t) - f_\alpha^{\mathrm{eq}}(\mathbf{r}, t)\right] + \delta_t F_\alpha, \tag{13}$$

where $\mathbf{r}$ is the position vector, δ_t the time step, τ_ν the dimensionless relaxation time which is a function of the fluid viscosity,

$$\tau_\nu = 3\nu\frac{\delta_t}{\delta_x^2} + 0.5, \tag{14}$$

where ν is the kinetic viscosity and δ_x the lattice constant (or grid size).

For electrokinetic flows in dilute electrolyte solutions, the external electrical force in Eq. (2) can be simplified to

$$\mathbf{F}_{\mathrm{E}} = \rho_e\mathbf{E} - \rho_e\nabla\Phi, \tag{15}$$

where Φ is the stream electrical potential caused by the ion movements in the solution based on the Nernst–Planck theory. Generally, the stream potential dominates the electro-viscosity effect in pressure driven flows, but its value is much less than the external potential and can be ignored in electrically driven flows. Therefore, the external force in the discrete lattice Boltzmann equation should include the pressure and electric force

$$F_\alpha = \frac{(-\nabla P + \rho_e\mathbf{E} - \rho_e\nabla\Phi)\cdot(\mathbf{e}_\alpha - \mathbf{u})}{\rho RT} f_\alpha^{\mathrm{eq}}. \tag{16}$$

The macroscopic density and velocity can be calculated using

$$\rho = \sum_\alpha f_\alpha, \tag{17}$$

$$\rho\mathbf{u} = \sum_\alpha \mathbf{e}_\alpha f_\alpha. \tag{18}$$

2.2.2. Evolution equation for electrodynamics

Borrowing the spirit from the lattice Boltzmann method, we rewrite Eq. (6) as a Boltzmann-like equation by expanding a time-dependent term:

$$\frac{\partial\psi}{\partial t} = \nabla^2\psi + g_{\mathrm{rhs}}(\mathbf{r}, \psi, t), \tag{19}$$

where

$$g_{\mathrm{rhs}} = \frac{1}{\varepsilon\varepsilon_0}\sum_i z_i e n_{i,\infty} \exp\left(-\frac{z_i e}{k_{\mathrm{B}}T}\psi\right)$$

represents the negative right-hand side (RHS) term of the original Poisson–Boltzmann equation. The solution of Eq. (6) is actually the steady solution of Eq. (18). The evolution equation for the electrical potential on the two-dimensional discrete lattices can then be written as [46]

$$g_\alpha(\mathbf{r} + \Delta\mathbf{r}, t + \delta_{t,g}) - g_\alpha(\mathbf{r}, t) = -\frac{1}{\tau_g}\left[g_\alpha(\mathbf{r}, t) - g_\alpha^{\mathrm{eq}}(\mathbf{r}, t)\right] + \left(1 - \frac{0.5}{\tau_g}\right)\delta_{t,g}\omega_\alpha g_{\mathrm{rhs}}, \tag{20}$$

where the equilibrium distribution of the electric potential evolution variable g is $g_\alpha^{\mathrm{eq}} = \varpi_\alpha \psi$, with

$$\varpi_\alpha = \begin{cases} 0, & \alpha = 0, \\ 1/6, & \alpha = 1, 2, 3, 4, \\ 1/12, & \alpha = 5, 6, 7, 8. \end{cases} \tag{21}$$

The time step in Eq. (20) is

$$\delta_{t,g} = \frac{\delta_x}{c'}, \tag{22}$$

where c' is a pseudo sound speed in the potential field [46]. The dimensionless relaxation time for Eq. (20) is

$$\tau_g = \frac{3\chi\delta_{t,g}}{2\delta_x^2} + 0.5, \tag{23}$$

where χ is defined as the potential diffusivity which equals to unity in these simulations.

The evolution equations (20)–(23) were proved consistent with the macroscopic nonlinear Poisson–Boltzmann equation (6). After evolving on the discrete lattices, the macroscopic electrical potential can be calculated using

$$\psi = \sum_\alpha (g_\alpha + 0.5\delta_{t,g} g_{\mathrm{rhs}} \omega_\alpha). \tag{24}$$

Though the electrical potential evolution equations are in an un-steady form, only the steady state result is realistic, because the electromagnetic susceptibility has not been considered. Although the lattice evolution method for nonlinear Poisson equation is not as efficient as the multi-grid solutions due to its long wavelength limit, it has the advantages of suitability for complex geometries and parallel computing. Although this paper only presents 2D cases, the algorithm is easy to extend to 3D cases [46].

2.2.3. Boundary conditions

The hydrodynamic boundary conditions for the lattice Boltzmann method have been studied extensively [58–66]. In the previous work for electrokinetic flows, the bounce-back rules were used [39–42,45–47], or a second-order accurate nonslip boundary condition was implemented at wall surfaces [49]. The half-way bounce-back rule [62,63] for the nonequilibrium distribution proposed by Zou and He [64] is introduced into this work and extended to both hydrodynamic and electrodynamic boundary implements to deal with the complex geometries in porous media.

At the boundary the following hydrodynamic boundary condition holds:

$$f_\alpha^{\mathrm{neq}} = f_\beta^{\mathrm{neq}}, \tag{25}$$

where the subscripts α and β represent opposite directions. Analogously, the nonequilibrium "bounce-back" rule for the electric potential distribution at the wall surfaces is suggested as

$$g_\alpha^{\mathrm{neq}} = -g_\beta^{\mathrm{neq}}.$$

The "half-way" bounce-back scheme with interpolation is used here to deal with the curved surfaces in porous media [65,66]. This boundary treatment has a super-linear accuracy when the wall surface varies between two adjacent nodes and an approximately second-order accuracy if the wall surface locates at the middle [63,64]. This method is easy to implement for complicated boundary conditions without special considerations for corners. Periodic conditions were implemented at the inlet and outlet.

3. Results and discussion

Fig. 1 shows a typical illustration of electrokinetic flows in structured porous media packed in a microchannel. Both channel walls and the particle surfaces are charged. The electrolyte solution is driven flow by an external electric field, a pressure drop or both effects. In this section, we will simulate the electrokinetic pumping effects in charged porous media using the mesoscopic evolution numerical methods described in Section 2. The effects of particle size, ionic concentration, external electric field strength, and particle surface zeta potential on the electrokinetic pump performance are analyzed.

In the following two dimensional simulations, the channel walls are homogeneously charged with the zeta potential $\zeta_w = -50$ mV. The channel width H is 1 μm. The charged microspheres are arranged as a structured array with equal space between in the channel. The particle diameter d_p varies from 54 to 325 nm, with remaining the porosity as a constant at 0.33. The particle surfaces are homogeneously charged, whose potentials ζ_p vary from −10 to −90 mV. The electrolyte solution is driven flowing through the porous media, whose properties are: the relative dielectric constant $\varepsilon = 81$, the density $\rho = 1000\ \mathrm{kg/m^3}$ and the dynamic viscosity $\mu = 0.889$ mPa s. The bulk ionic concentration c_∞ changes from 10^{-6} to 10^{-3} M and the external electric field strength E changes from 1 to 5 kV/m.

3.1. Particle size effects

The effects of particle size on the electric potential distribution are first considered. In most previous analytical or numerical modeling of electroosmosis in porous media, the electric double layer (EDL) was mostly assumed small compared to the particle size so that the Debye–Huckle theory would lead to

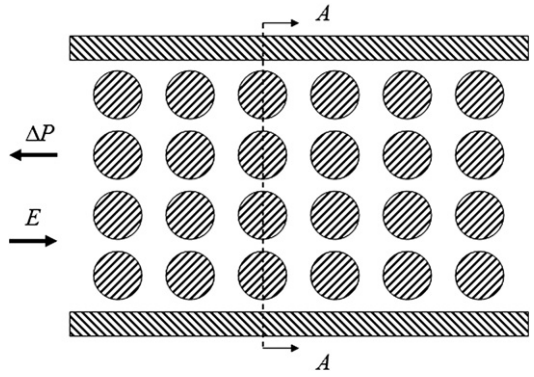

Fig. 1. Schematic illustration of electrokinetic flow in a microchannel packed with charged porous media. The A–A section crosses the centers of the cycles in the same section.

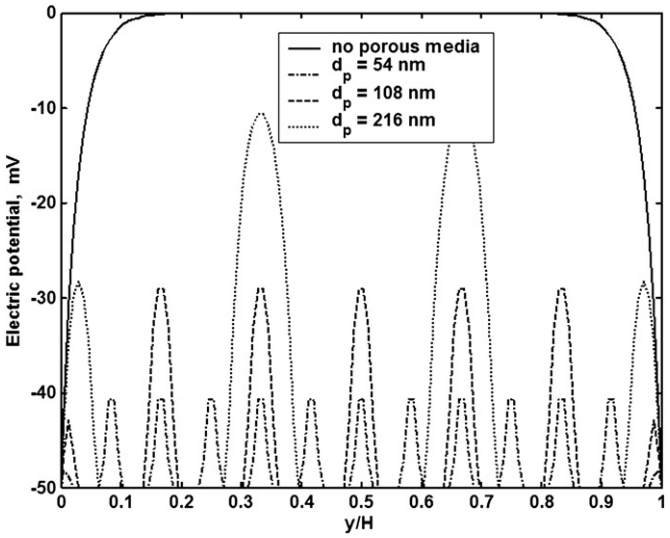

Fig. 2. The electric potential and velocity profiles across the A–A section for different particle sizes.

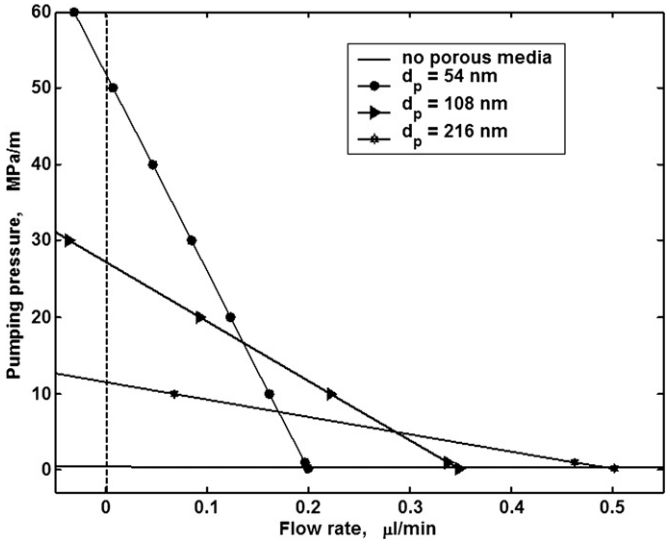

Fig. 3. Backpressure vs flow rate for different particle sizes.

simplified expressions for electric potential and velocity fields [18–20]. However when the particle size is of the same level as or even smaller than the EDL thickness, the particle surface potential will affect greatly on the bulk electric potential distribution, not only on the boundary conditions. Fig. 2 shows the electric potential profiles across the A–A section for different particle sizes. Because the particle diameter and the gap distance are both comparable to the EDL thickness, the electric potential distribution is significantly affected by the particle surface charge. The electric potential profile in a channel packed with charged porous media is quite different from that in a vacant channel. Smaller particles lead to smaller electric potential maximums across the channel.

Since the porous media additive has been reported to improve performances of the electroosmotic micropump, the nanoscale particle size effects on the pumping performance are here investigated. Fig. 3 shows the backpressure versus flow rate for different particle sizes when $E = 1$ kV/m, $\zeta_p = -50$ mV, and $c_\infty = 10^{-4}$ M. Comparing with the no porous media additivity case, the porous media additivity improves the pump performance significantly with much higher pumping pressures and lower flow rates. A smaller particle size leads to a higher backpressure maximum and a lower zero-pressure-drop flow rate. Under the current parameters and conditions the backpressure maximum reaches over 50 MPa/m for $d_p = 54$ nm. For each case, the pressure and flow rate are in a linear relationship, which agrees with the experimental data in Ref. [18].

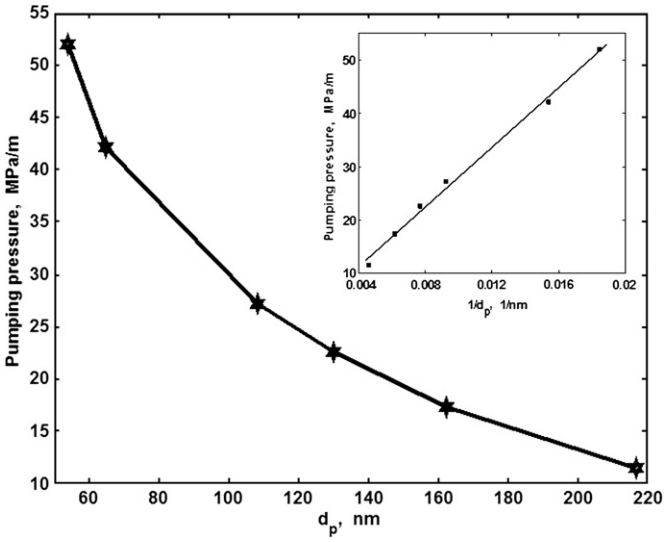

Fig. 4. Maximum pumping pressure vs particle diameter.

The maximum pumping pressure for each case can be obtained from the intercept of the pressure-flow rate curve on y-axis. The curves of the maximum pumping pressure versus particle diameters are plotted in Fig. 4. The results indicate that the smaller the particle diameter, the higher the maximum pumping pressure. The subplot in Fig. 4 shows the maximum pumping pressure is almost inversely proportional to the particle diameter. This result disagrees with the macroscopic linearized analytical solution which results in a maximum pumping pressure depending on the inverse square of particle diameter [18]. The reason lies in that the surface electric potentials of nanoscale particles change the bulk potential distribution and the consequent driving force differently from those of macroscale ones do.

In macroscale analyses, the flow rate is independent of particle size for given structural parameters of porosity and tortuosity [18]. However, things change for nanoscale. Fig. 5 shows pumping flow rate versus particle size when $E = 1$ kV/m, $\Delta P = 0$ Pa/m, $\zeta_p = -50$ mV, and $c_\infty = 10^{-4}$ M. The flow rate increases sharply with the particle size when the particle is smaller than 160 nm and a little platter when the particle becomes bigger. For macroscale cases, the variety of particle size only changes locations of the boundaries but never changes the shape and maximum value of the electric potential profiles under the thin EDL assumption; however for nanoscale, the particle size variety does not only change the maximum electric

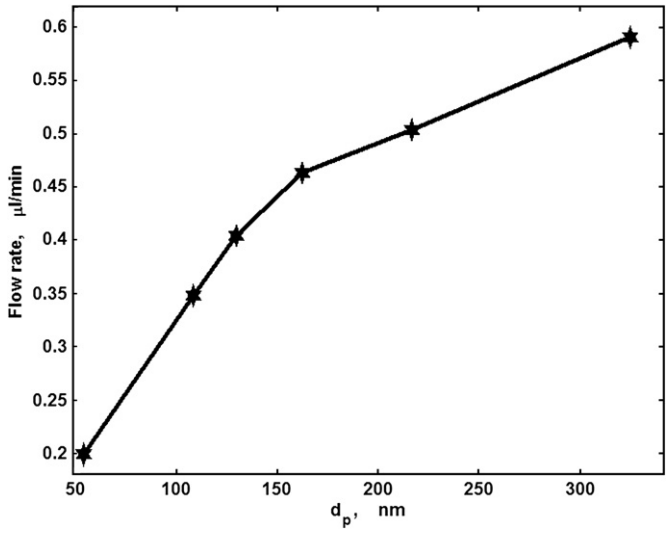

Fig. 5. Flow rate vs particle diameter under zero pressure drop.

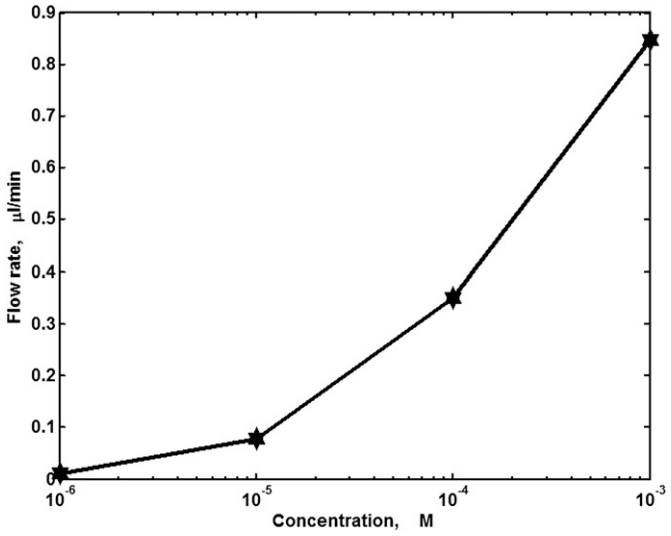

Fig. 7. Flow rate vs bulk ionic concentration.

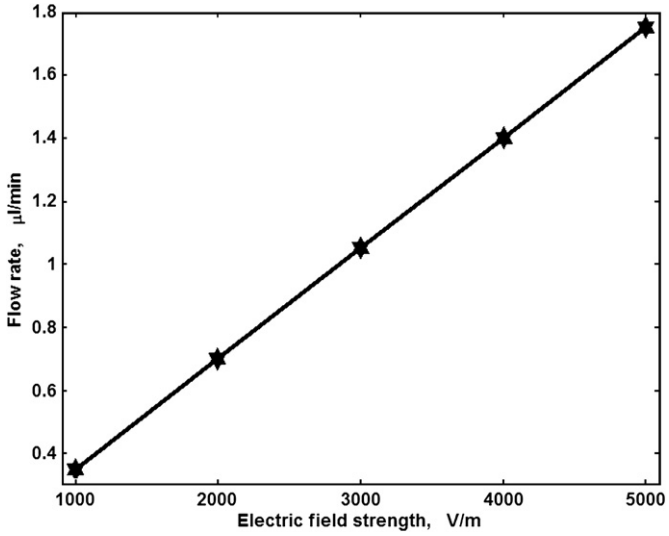

Fig. 6. Flow rate vs external electric field strength.

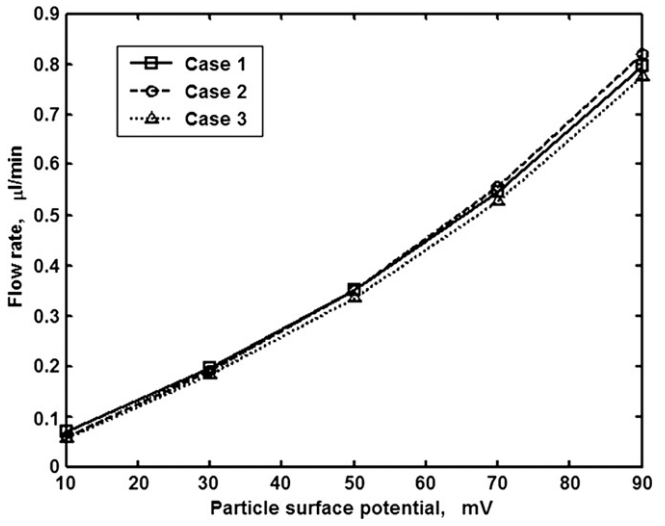

Fig. 8. Flow rate vs particle surface potential for three charged schemes. Case 1: the wall surface potential changes with the particle surface potential synchronously; case 2: the wall surface potential remains $\zeta_w = -50$ mV unchanged; case 3: the wall surface potential remains uncharged ($\zeta_w = 0$ mV).

potential but also changes the profile shape, as shown in Fig. 2. This is why the current results disagree with the macroscale predictions. This result also suggests that fine porous media can be used to control electric fluids precisely.

3.2. External electric field strength effect

The dependence of flow rate on external electric field strength for the electroosmotic pump is also numerically studied when $\Delta P = 0$ Pa/m, $\zeta_p = -50$ mV, $d_p = 108$ nm, and $c_\infty = 10^{-4}$ M. Fig. 6 shows a perfect linearity between the flow rate and the electric field strength, which agrees well with the experimental data [18].

3.3. Ionic concentration effect

Since the ionic concentration has a great effect on the electric potential distribution in microchannels [46], here we model the flow rate versus the ionic concentration in an electroosmotic micropump packed by nanoscale charged porous media when $E = 1$ kV/m, $\Delta P = 0$ Pa/m, $\zeta_p = -50$ mV, and $d_p = 108$ nm. Fig. 7 indicates the flow rate increases with the ionic concentration monotonically.

3.4. Surface potential effect

The effect of particle surface potentials on pumping flow rate is studied by changing the particle surface potential from -10 to -90 mV. Here we consider three cases: case 1, the wall surface potential changes with the particle surface potential synchronously; case 2, the wall surface potential remains $\zeta_w = -50$ mV; case 3, the wall surface potential remains uncharged ($\zeta_w = 0$ mV). Fig. 8 compares the results of the three cases where $E = 1$ kV/m, $\Delta P = 0$ Pa/m, $c_\infty = 10^{-4}$ M, and $d_p = 108$ nm. The results indicate that the flow rate increases

with the particle surface potential, however with little dependence of the wall surface potential. The relative error between each case is less than 5% when the particle surface potential is larger than 30 mV, which indicates that the main driving force of the electroosmotic pump comes from the charged porous media rather than the channel walls.

4. Conclusions

The mesoscopic evolution methods developed in this paper provide an efficient numerical tool to analyze the electrokinetic transport characteristics in nanoscale charged porous media where the particle surface potential influences greatly the bulk electric potential distribution. The results indicate: the particle size affects not only the electric potential maximum but also the shape of the electric potential profile across the channel. As a result, for a certain porosity the maximum pumping pressure is inversely proportional to the particle diameter rather than the inverse square of the particle diameter based on the linearization assumption and the flow rates increase with the particle size rather than keep constant as predicted by the macroscopic analyses. The flow rate changes linearly with the backpressure and the external electric field strength, which agrees well with the existing experimental data. The results also show that the flow rate is dependent greatly on the ionic concentration and the particle surface potential, however slightly affected by the electric potential of channel walls. The current results may improve the understanding of the electrokinetic transport characteristics in nanoscale charged porous media in microchannels.

Acknowledgments

This work was supported by the National Natural Science Foundation of China (Grant No. 59995550-2) and the National Textile Center (NTC) M04-CD01. The authors would like to thank Profs. J.C. Xu, C. Yang, D.Q. Li, and Z.X. Li for helpful discussions.

References

[1] R.E. Oosterbroek, A. van den Berg, Lab-On-A-Chip: Miniaturized Systems for (Bio) Chemical Analysis and Synthesis, Elsevier, Boston, 2003.
[2] K.A. Sharp, B. Honig, Annu. Rev. Biophys. Biophys. Chem. 19 (1990) 301–332.
[3] P.K. Wong, J.T. Wang, J.H. Deval, C.M. Ho, IEEE/ASME Trans. Mechantron. 9 (2004) 366–376.
[4] C.Y. Wang, Chem. Rev. 104 (2004) 4727–4766.
[5] C.M. Ho, Y.C. Tai, Annu. Rev. Fluid Mech. 30 (1998) 579–612.
[6] M. Wang, Z.X. Li, Instrum. Techn. Sens. 7 (2002) 1–4.
[7] D.J. Laser, J.G. Santiago, J. Micromech. Microeng. 14 (6) (2004) R35–R64.
[8] Z.X. Li, M. Wang, L.Y. Tan, Chin. Sci. Bull. 47 (2002) 518–522.
[9] Z.X. Li, M. Wang, X.B. Yao, Z.Y. Guo, Microscale Thermophys. Eng. 8 (1) (2004) 31–42.
[10] Z.Z. Yin, A. Prosperetti, J. Micromech. Microeng. 15 (9) (2005) 1683–1691.
[11] H.A. Stone, A.D. Stroock, A. Ajdari, Annu. Rev. Fluid Mech. 36 (2004) 381–411.
[12] R. Karnik, R. Fan, M. Yue, D.Y. Li, P.D. Yang, A. Majumdar, Nano Lett. 5 (5) (2005) 943–948.
[13] A. Brask, G. Goranovic, M.J. Jensen, H. Bruus, J. Micromech. Microeng. 15 (4) (2005) 883–891.
[14] M.Z. Bazant, T.M. Squires, Phys. Rev. Lett. 92 (2004) 066101.
[15] M.H. Oddy, J.G. Santiago, J.C. Mikkelsen, Anal. Chem. 73 (2001) 5822–5832.
[16] E. Biddiss, D. Erickson, D.Q. Li, Anal. Chem. 7 (11) (2004) 3208–3213.
[17] D.J. Throckmorton, T.J. Shepodd, A.K. Singh, Anal. Chem. 74 (4) (2002) 784–789.
[18] S.L. Zeng, C.H. Chen, J.C. Mikkelsen, J.G. Santiago, Sens. Actuators B Chem. 79 (2–3) (2001) 107–114.
[19] S.H. Yao, J.G. Santiago, J. Colloids Surf. 268 (1) (2003) 133–142.
[20] J.A. Tripp, F. Svec, J.M.J. Frechet, S.L. Zeng, J.C. Mikkelsen, J.G. Santiago, Sens. Actuators B Chem. 99 (1) (2004) 66–73.
[21] F.C. Leinweber, J.C.T. Eijkel, J.G. Bomer, A. van den Berg, Anal. Chem. 78 (2006) 1425–1434.
[22] D. Coelho, M. Shapiro, J.F. Thovert, P.M. Adler, J. Colloid Interface Sci. 181 (1) (1996) 169–190.
[23] M.R. Schure, R.E. Murphy, W.L. Klotz, W. Lau, Anal. Chem. 70 (23) (1998) 4985–4995.
[24] S. Marino, D. Coelho, S. Bekri, P.M. Adler, J. Colloid Interface Sci. 223 (2) (2000) 292–304.
[25] P.M. Adler, V. Mityushev, J. Phys. A Math. Gene. 36 (2) (2003) 391–404.
[26] Y.J. Kang, C. Yang, X.Y. Huang, Int. J. Eng. Sci. 42 (2004) 2011–2027.
[27] B. Honig, A. Nicholls, Science 268 (5214) (1995) 1144–1149.
[28] S.A. Allison, Macromolecules 29 (23) (1996) 7391–7401.
[29] D. Hlushkou, A. Seidel-Morgenstern, U. Tallarek, Langmuir 21 (13) (2005) 6097–6112.
[30] C. Yang, D.Q. Li, Colloids Surf. A 143 (1998) 339–353.
[31] D.Q. Li, Colloids Surf. A 195 (2001) 35–57.
[32] J. Lee, Y. Hu, D.Q. Li, Anal. Chem. Acta 543 (2005) 99–108.
[33] C. Ye, D.Q. Li, J. Colloid Interface Sci. 272 (2004) 480–488.
[34] Y.D. Hu, C. Werner, D.Q. Li, Anal. Chem. 75 (2003) 5747–5758.
[35] Y.D. Hu, C. Werner, D.Q. Li, J. Colloid Interface Sci. 280 (2004) 527–536.
[36] R.J. Flatt, P. Bowen, Cem. Concr. Res. 33 (2003) 781–791.
[37] X.Y. He, N. Li, Comput. Phys. Commun. 129 (2000) 158–166.
[38] J. Horbach, D. Frenkel, Phys. Rev. E 64 (2001) 061507.
[39] B. Li, D.Y. Kwok, Langmuir 19 (7) (2003) 3041–3048.
[40] B. Li, D.Y. Kwok, J. Chem. Phys. 120 (2004) 947–953.
[41] F.Z. Tian, B.M. Li, D.Y. Kwok, Lattice Boltzmann simulation of electroosmotic flows in micro- and nanochannels, in: International Conference on MEMS, NANO and Smart Systems (ICMENS), Banff, Alberta, Canada, 2004, pp. 294–299.
[42] S. Melchionna, S. Succi, J. Chem. Phys. 120 (2004) 4492–4497.
[43] J. Wu, V. Srinivasan, J. Xu, C.Y. Wang, J. Electrochem. Soc. 149 (10) (2002) A1342–A1348.
[44] J.C. Xu, personal communications, 2005 and 2006.
[45] Z.L. Guo, T.S. Zhao, Y. Shi, J. Chem. Phys. 112 (14) (2005) 144907.
[46] J.K. Wang, M. Wang, Z.X. Li, J. Colloid Interface Sci. 296 (2) (2006) 729–736.
[47] M. Wang, J.K. Wang, Z.X. Li, J. Colloid Interface Sci. 300 (1) (2006) 446.
[48] J.K. Wang, M. Wang, Z.X. Li, Mod. Phys. Lett. B 19 (2005) 1515–1518.
[49] M. Wang, J.K. Wang, S.Y. Chen, J. Comput. Phys. (2006).
[50] P.H. Wiersema, A.L. Loeb, J.Th.G. Overbeek, J. Colloid Interface Sci. 22 (1) (1966) 78–99.
[51] R.W. O'Brien, L.R. White, J. Chem. Soc. Faraday Trans. II 74 (1978) 1607–1626.
[52] J.H. Masliyah, S. Bhattacharjee, Electrokinetic and Colloid Transport Phenomena, Wiley, Hoboken, 2006.
[53] D.Q. Li, Electrokinetics in Microfluidics, Academic Press, Oxford, 2004.
[54] S.Y. Chen, G.D. Doolen, Annu. Rev. Fluid Mech. 30 (1998) 329–364.
[55] X.Y. He, L.S. Luo, Phys. Rev. E 56 (6) (1997) 6811–6817.
[56] X.Y. He, S.Y. Chen, G.D. Doolen, J. Comput. Phys. 42 (146) (1998) 282–300.
[57] Y.H. Qian, D. Dhumieres, P. Lallemand, Europhys. Lett. 17 (1992) 479–484.
[58] D.R. Noble, S.Y. Chen, J.G. Georgiadis, R.O. Buckius, Phys. Fluids 7 (1) (1995) 203–209.

[59] T. Inamuro, M. Yoshino, F. Ogino, Phys. Fluids 7 (12) (1995) 2928–2930; Erratum. T. Inamuro, M. Yoshino, F. Ogino, Phys. Fluids 8 (4) (1996) 1124.
[60] S.Y. Chen, D. Martinez, R.W. Mei, Phys. Fluids 8 (9) (1996) 2527–2536.
[61] M. Bouzidi, M. Firdaouss, P. Lallemand, Phys. Fluids 13 (2002) 3452–3459.
[62] D.P. Ziegler, J. Statist. Phys. 71 (5/6) (1993) 1171–1177.
[63] M. Rohde, D. Kandhai, J.J. Derksen, H.E.A. van den Akker, Phys. Rev. E 67 (6) (2003) 066703.
[64] Q.S. Zou, X.Y. He, Phys. Fluids 9 (6) (1997) 1591–1598.
[65] D. Yu, R. Mei, W. Shyy, L.S. Luo, Phys. Rev. E 65 (2002) 041203.
[66] P. Lallemand, L.S. Luo, J. Comput. Phys. 184 (2) (2003) 406–421.